Supplementary Information

A Vaccine of Photodynamic Immunogenic Cell Death: Tumor Cell Caged by Cellular Disulfide/Thiol Exchange for Immunotherapy

Ya Wen,[†a] Yiqiong Liu,[†a] Fangfang Guo,[a] Yi Han,[a] Qiansai Qiu,[c] Yan Li,[a] Haiqing Dong,*[b] Tianbin Ren,[a] and Yongyong Li*[a]

[a.] Shanghai Tenth People's Hospital, The Institute for Biomedical Engineering and Nano Science, Tongji University School of Medicine, Shanghai 200092, P. R. China. E-mail: yongyong_li@tongji.edu.cn

[b.] Key Laboratory of Spine and Spinal Cord Injury Repair, and Regeneration of Ministry of Education, Orthopaedic Department of Tongji Hospital, Tongji University School of Medicine, Shanghai 200092, P. R. China. E-mail: inano_donghq@tongji.edu.cn

[c.] Department of Medical Imaging, Nantong Tumor Hospital, Nantong University, Nantong 226361, P. R. China

[†] These authors contributed equally to this study.

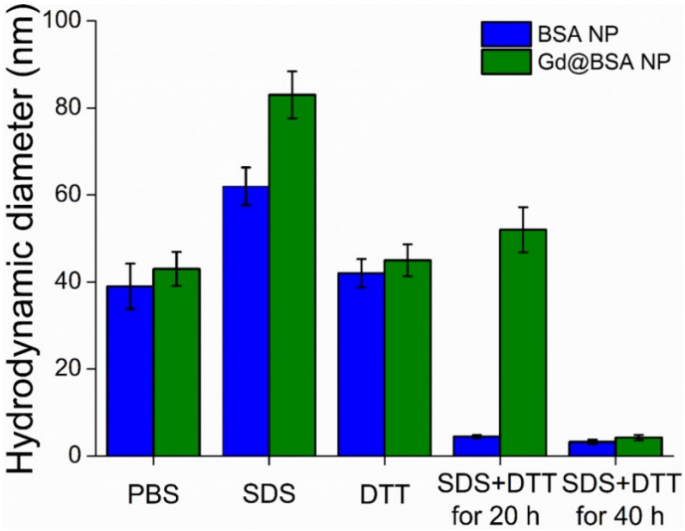

Fig. S1 Effects of 1 % SDS (destroyer of hydrophobicity) and 30 mM DTT (destroyer of disulfide) on the hydrodynamic diameter of BSA NP and Gd@BSA NP at predetermined time points.

To elucidate the intermolecular forces stabilizing the nanoparticles, both BSA NPs and Gd@BSA NPs were treated with SDS and DTT, an effective destroyer of hydrophobic interaction and disulfide bonds respectively. As exhibited in Fig. S1, SDS or DTT alone could not dissociate the nanoparticles since their size were maintained after treatment. However, if they were co-treated with SDS in combination with DTT, there appeared a complete dissociation with sharp decrease in size. This indicates the existence of synergistic physical and chemical forces in stabilizing the nanoparticles. Interestingly, integration of Gd could further improve the stability since the size of Gd@BSA NPs endured a longer duration in the dissociated condition.

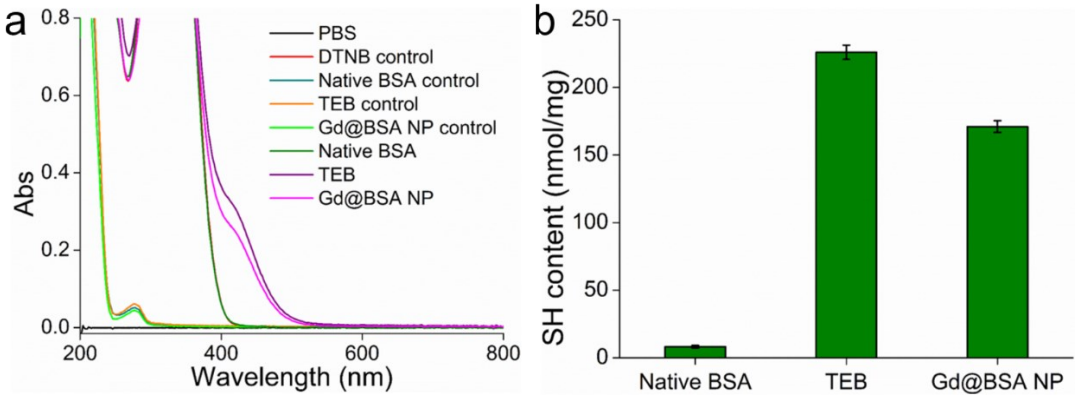

Fig. S2 (a) The UV absorbance at 412 nm of TNB, the reaction product of native BSA, TEB or Gd@BSA NP with DTNB, for the determination of thiol (SH) content. (b) SH content of native BSA, TEB and Gd@BSA NP.

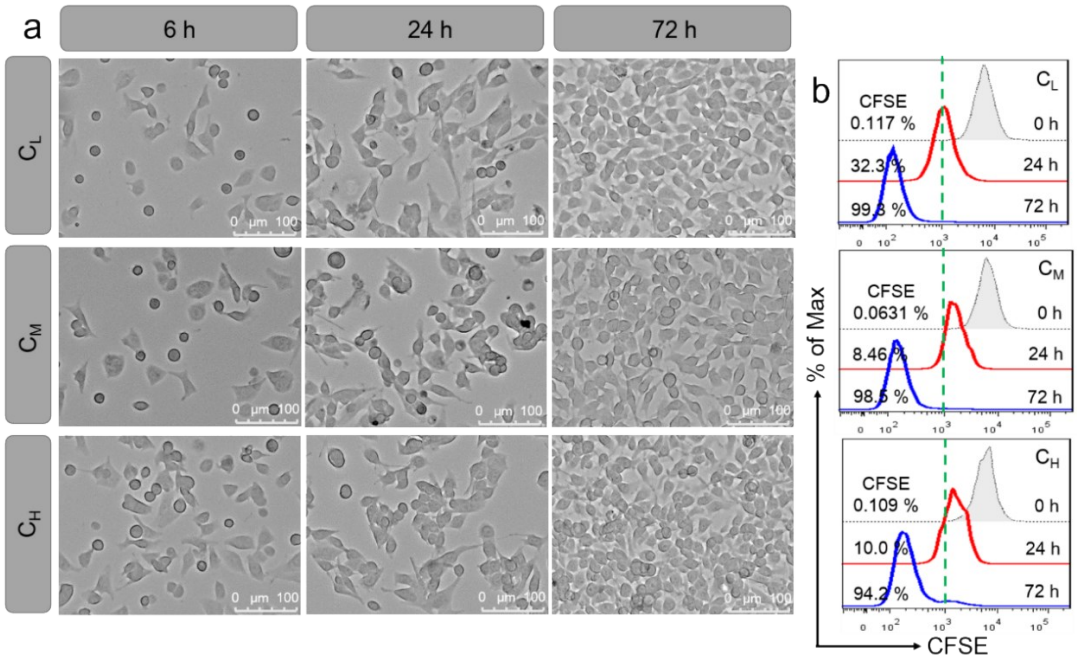

Fig. S3 Division and proliferation profile of TABN surface-anchored B16F10 cells. (a) The growth behavior of TABN surface-anchored B16F10 cells treated with different NP concentrations in 72 h observed by optical microscope. (b) The corresponding propagation property of TABN surface-anchored B16F10 cells investigated with flow cytometer by measuring the fluorescence intensity of CFSE pre-labeled to native B16F10 cells.

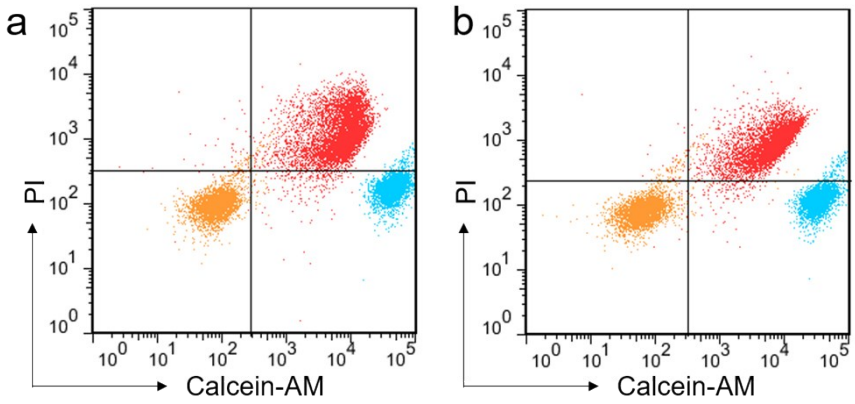

Fig. S4 Flow cytometry of caged tumor cell (red), native cell (blue) and blank cell (yellow) at 0 h (a) and 24 h (b), which was stained with calcein-AM (live) and PI (dead).

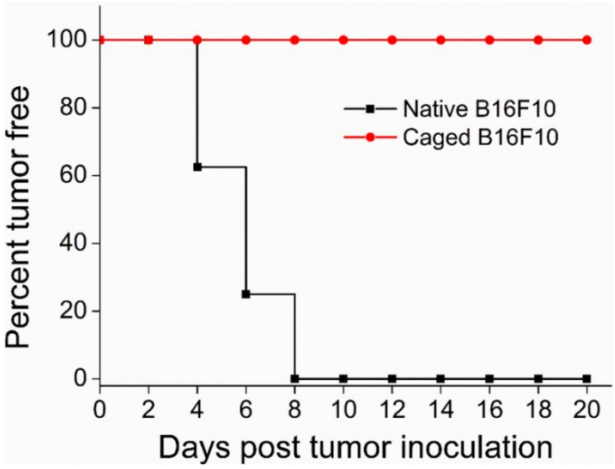

Fig. S5 Evaluation of tumorigenicity of caged B16F10 (C_H) cells by subcutaneously inoculating therapeutic dose of caged cells (2×10^6 cells) (n = 8).

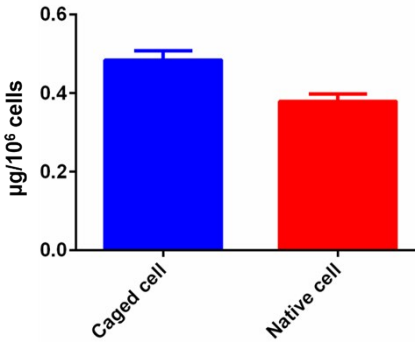

Fig. S6 The Ce6 loading capacity of tumor cell in the presence/absence of cage.

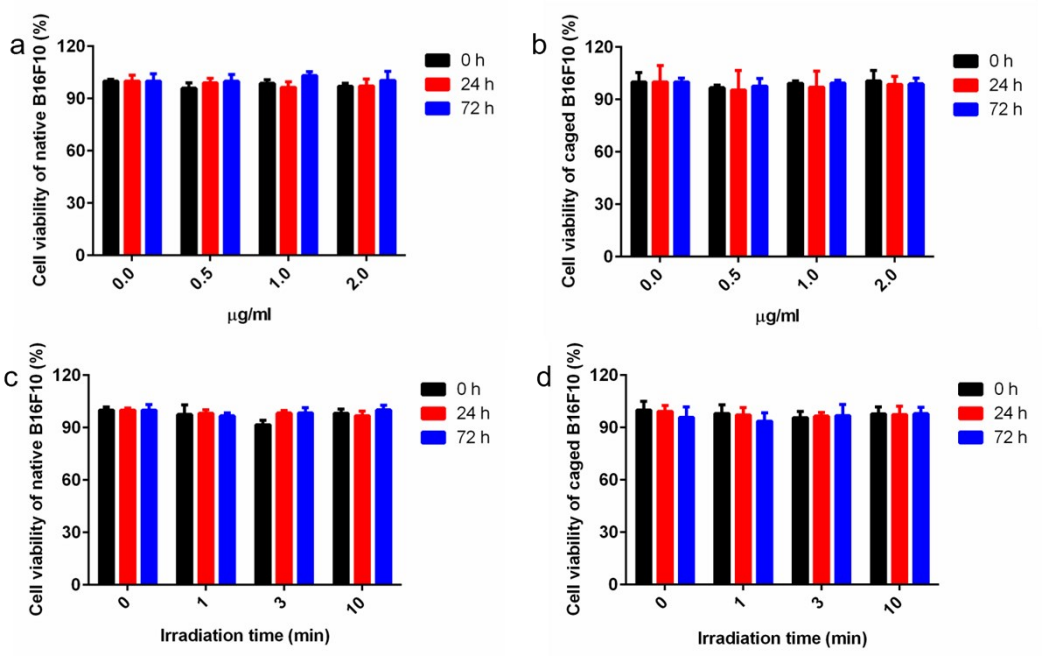

Fig. S7 (a, b) Toxicity of Ce6 to native and caged cells at the concentration of 0.5, 1.0, 2.0 μg/ml in the absence of irradiation. (c, d) Toxicity of irradiation to native and caged cells at the time of 1, 3, 10 min in the absence of Ce6 at 0, 24, 72 h.

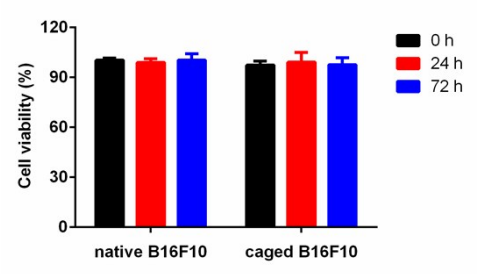

Fig. S8 The native and caged B16F10 were separately as the normalization control (100%) for Fig. 4b and 4c.

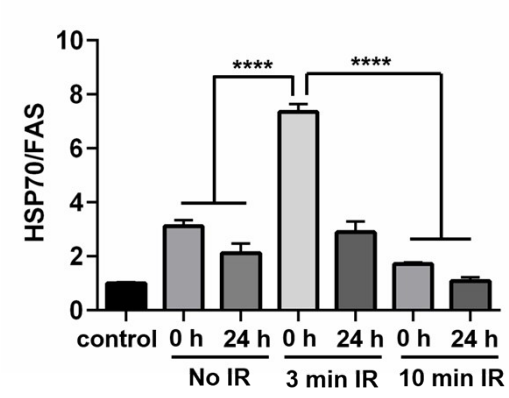

Fig. S9 Quantification and statistical analysis of HSP70 expression (IR, irradiation).

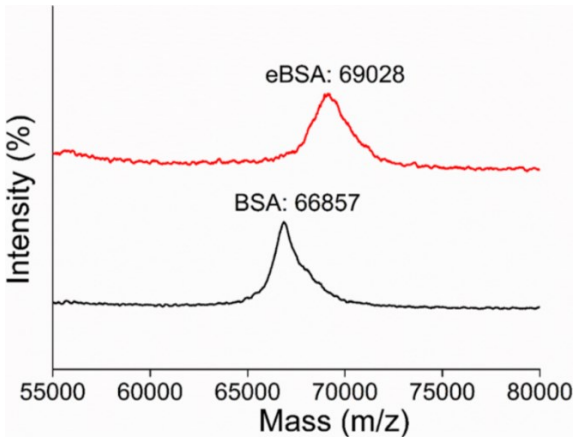

Fig. S10 Mass spectrometry to characterize the modification of BSA with ethylenediamine.

Cationic BSA (eBSA) was synthesized by ethylenediamine modification to BSA through condensation reaction between amidogen and carboxyl and the mass spectrometric analysis indicated ~ 51 ethylenediamine molecules were conjugated to one BSA molecule (Fig. S5).

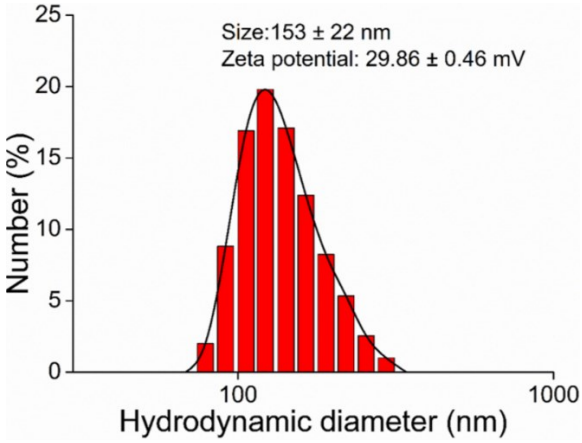

Fig. S11 Hydrodynamic diameter and zeta potential of CpG@eBSA NP (W_{eBSA} : W_{CpG} = 20 : 1).

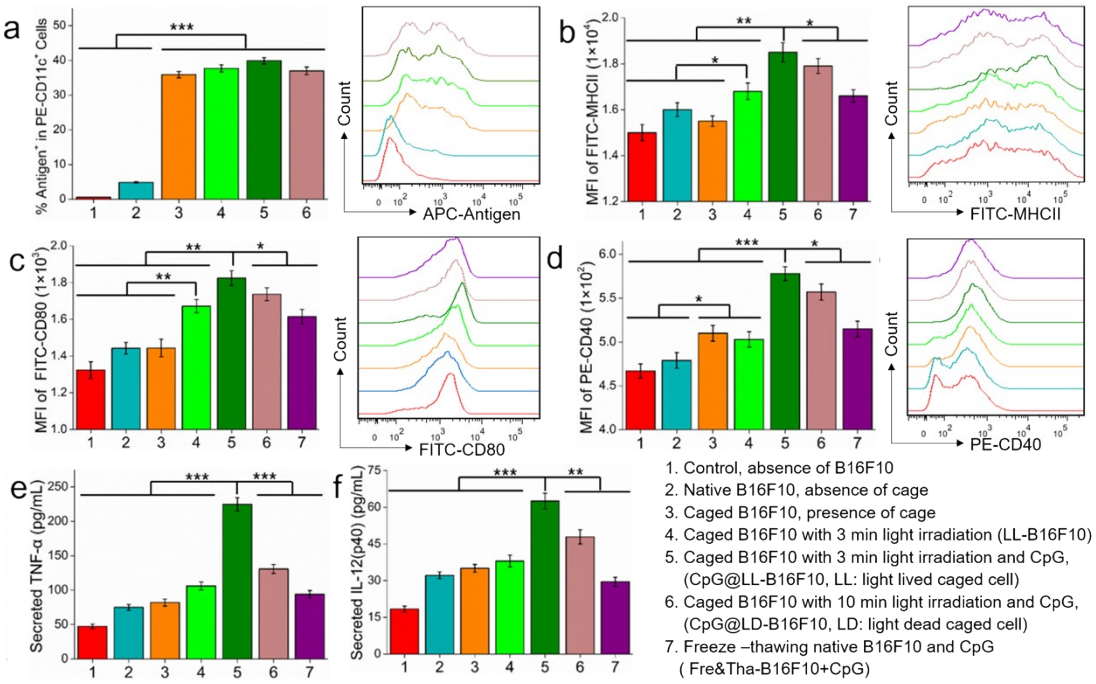

Fig. S12 Photoactivated CLCV activates DC in vitro. (a) Phagocytosis of caged tumor cells by BMDCs. Measurement of costimulatory markers MHCII (b), CD80 (c) and CD40 (d) to characterize the maturation of BMDCs post 12 h vaccine stimulation. Equivalent freeze-thawing B16F10 cells mixed with CpG (Fre&Tha-B16F10 + CpG) were served as the control. Amount of (e) TNF-α and (f) IL-12(p40) in BMDC supernatant after 12 h stimulation with the vaccines measured by ELISA. Data are presented as mean ± SD (n = 3). * $P < 0.05$, ** $P < 0.01$, *** $P < 0.001$.

Internalized or surface adsorbed Ce6 in live B16F10 or other vaccine formulations was used for detection by flow cytometry. The results demonstrated the cage process and photodynamic treatment significantly improved the phagocytosis efficiency by BMDCs (~ 7-fold higher than live tumor cells). In contrast, live B16F10 only exhibited a weak phagocytosis (Fig. S7a). The maturation of BMDCs was measured after 12 h vaccine stimulation, with equivalent freeze-thawing B16F10 cells mixed with CpG (Fre&Tha-B16F10 + CpG) as the control. Indeed, the cage process and light treatment were able to upregulate costimulatory markers, such as MHCII (Fig. S7b), CD80 (Fig. S7c) and CD40 (Fig. S7d). CpG formulation could further potentiate the maturation indices. Similarly, the cage process and light treatment promoted the secretion of inflammatory cytokines from BMDCs, including TNF-α (Fig. S7e) and IL-12(p40) (Fig. S7f). Overall, light triggered immunogenic expression of HSP70 on caged cell surface was crucial for strong DC maturation and cytokine secretion.